Title	Engineering the growth of germanium nanowires by tuning the supersaturation of Au/Ge binary alloy catalysts
Authors	O'Regan, Colm;Biswas, Subhajit;O'Kelly, Curtis;Jung, Soon Jung;Boland, John J.;Petkov, Nikolay;Holmes, Justin D.
Publication date	2013-07-08
Original Citation	O'REGAN, C., BISWAS, S., O'KELLY, C., JUNG, S. J., BOLAND, J. J., PETKOV, N. & HOLMES, J. D. 2013. Engineering the Growth of Germanium Nanowires by Tuning the Supersaturation of Au/Ge Binary Alloy Catalysts. Chemistry of Materials, 25, 3096-3104. http://dx.doi.org/10.1021/cm401281y
Type of publication	Article (peer-reviewed)
Link to publisher's version	http://pubs.acs.org/journal/cmatex - 10.1021/cm401281y
Rights	© 2013 American Chemical Society. This document is the Accepted Manuscript version of a Published Work that appeared in final form in Chemistry of Materials, copyright © American Chemical Society after peer review and technical editing by the publisher. To access the final edited and published work see http://dx.doi.org/10.1021/cm401281y
Download date	2025-04-17 08:35:40
Item downloaded from	https://hdl.handle.net/10468/2466

Engineering the Growth of Germanium Nanowires by Tuning the Supersaturation of Au/Ge Binary Alloy Catalysts

Colm O'Regan[†,ϕ], *Subhajit Biswas* [†,ϕ], *Curtis O'Kelly*[§,ϕ], *Soon Jung Jung*[§,ϕ], *John J. Boland*[§,ϕ], *Nikolay Petkov*[†,ϕ] *and Justin D. Holmes*[†,ϕ*]

[†]Materials Chemistry & Analysis Group, Department of Chemistry and the Tyndall National Institute, University College Cork, Cork, Ireland.

[ϕ]Centre for Research on Adaptive Nanostructures and Nanodevices (CRANN), Trinity College Dublin, Dublin 2, Ireland.

[§]School of Chemistry, Trinity College Dublin, Dublin 2, Ireland.

*To whom correspondence should be addressed: Tel: +353 (0)21 4903608; Fax: +353 (0)21 4274097; E-mail: j.holmes@ucc.ie

Abstract

The synthesis of Ge nanowires with very high-aspect ratios (greater than 1000) and uniform crystal growth directions is highly desirable, not only for investigating the fundamental properties of nanoscale materials, but also for fabricating integrated functional nanodevices. In this article, we present a unique approach for manipulating the supersaturation, and thus the growth kinetics, of Ge nanowires using Au/Ge bilayer films. Ge nanowires were synthesized on substrates consisting of two parts: a Au film on one half of a Si substrate and a Au/Ge bilayer film on the other half of the

substrate. Upon annealing the substrate, Au and Au/Ge binary alloy catalysts were formed on the Au-side and Au/Ge-side of the substrates respectively, under identical conditions. The mean lengths of Ge nanowires produced were found to be significantly longer on the Au/Ge bilayer side of the substrate compared to the Au-coated side, as a result of a reduced incubation time for nucleation on the bi-layer side. The mean length and growth rate on the bilayer side (with a 1 nm Ge film) was found to be 5.5 ± 2.3 μm and 3.7×10^{-3} μm s^{-1} respectively, and 2.7 ± 0.8 μm and 1.8×10^{-3} μm s^{-1} for the Au film. Additionally, the lengths and growth rates of the nanowires further increased as the thickness of the Ge layer in the Au/Ge bilayer was increased. In-situ TEM experiments were performed to probe the kinetics of Ge nanowire growth from the Au/Ge bilayer substrates. Diffraction contrast during in-situ heating of the bilayer films clarified the fact that thinner Ge films, *i.e.* lower Ge concentration, take longer to alloy with Au than thicker films. Phase separation was also more significant for thicker Ge films upon cooling. The use of binary alloy catalyst particles, instead of the more commonly used elementary metal catalyst, enabled the supersaturation of Ge during nanowire growth to be readily tailored, offering a unique approach to producing very long high aspect ratio nanowires.

Keywords: Nanowires, germanium, vapor-liquid-solid growth, supersaturation, growth rate

Introduction

One-dimensional (1D) semiconductor nanowires have stimulated much interest in the last number of decades due to their potential use as building blocks for assembling nanoscale devices and architectures. [1-3] While Si has been the material of choice for many years for nanoscale electronic devices [1], there has recently been a renewed interest in Ge [4-7] for applications such as nano-electromechanical systems (NEMS) [8, 9], lithium-ion batteries [10-12], field effect transistors (FETs) [13] and photovoltaics [14]. Like Si, Ge is a Group 14 semiconductor material and exhibits certain properties that are superior to those of Si, including a higher charge carrier mobility [15] and a larger Bohr exciton radius, leading to more pronounced quantum confinement effects at higher dimensions.

[16] Notably, the many parallels between Si and Ge should allow the seamless integration of Ge into current Si based devices.

The vapor-liquid-solid (VLS) method is the most recognized approach for synthesizing Ge nanowires, allowing control over morphology and aspect ratio. The synthesis of high aspect ratio Ge nanowires with diameters between 10-20 nm and lengths in the micrometer and even millimeter regime, is of practical importance for the development of multiple device structures using individual nanowires. Long Ge nanowires, with high aspect ratios, can potentially be achieved by manipulating the rate determining step of VLS growth. Previous reports have highlighted that the incorporation of growth species (via the vapor phase) at the liquid-vapor interface [17-19] and the crystallization of nanowires at the liquid-solid interface [20] can both act as potential rate determining steps in the VLS mechanism. Whilst both the incorporation and crystallization steps play a role in determining the overall rate of nanowire growth, the incorporation process can be neglected in our VLS experiments as we assume the precursor pressure remains constant throughout the growth process; due to minimal temperature variations and carrying out reactions at atmospheric pressure. Therefore, assuming the crystallization of the Ge nanowires to be rate limiting, the enhanced rate of nanowire growth can be achieved by increasing the supersaturation of Ge in a binary system, such as Au-Ge. Supersaturation acts as the driving force for layer-by-layer crystallization at the triple phase boundary (TPB) during the nanowire growth process [21]. Han *et al.*[22] previously tuned the supersaturation of Au-Ga binary alloy particles in order to manipulate the growth of GaAs nanowires. They found that by increasing the Ga concentration in the seeds, by varying the thickness of the Au film deposited on SiO_2/Si substrates, they could increase the growth rate of the resulting nanowires and maintain unidirectional growth. Standard Au films have already been used to promote the growth of Ge nanowires by several groups [23-25]. Whilst Ge buffer films have been used to grow taper-free and highly crystalline Ge nanowires via a two-temperature process [26, 27] and have also been used to catalyze the growth of Au and Si_3Cu nanowires [28, 29], they have not been employed to manipulate the growth kinetics of Ge nanowire growth via a VLS process. Here, we

report the successful manipulation of the supersaturation in the liquid seeded bottom-up growth of Ge nanowires by tailoring the eutectic composition in Au-Ge bilayer films to influence the induction time for nanowire growth; providing a facile method for growing high aspect ratio Ge nanowires for future nanoscale devices.

Experimental

Si(100) substrates were coated with a 5 nm Au film using a Cressington HR 208 sputter coater with a quartz crystal thickness monitor. The target was placed inside the instrument and the pressure pumped down to 0.01 mbar. The density of Ge was then entered into the thickness monitor and the current set to 60 mA. Ar gas was then bled into the chamber. With the shutter closed, 1-2 nm of Ge was removed from the target to remove the surface oxide. The shutter was opened and the Ge deposited with the thickness being monitored in real time. Three samples consisting of a layer of Ge with thicknesses of 1, 2 and 5 nm were prepared by depositing such a layer on one half of the substrate, forming a Au/Ge bilayer. Diphenylgermane (DPG) was used as the precursor for Ge nanowire growth. Solutions of DPG in anhydrous toluene were prepared in an N_2 glove box with a typical concentration of 1.07×10^{-4} M. Continuous-flow reactions were carried out in a toluene medium using a liquid injection chemical vapor deposition (LICVD) methodology. The as-prepared Au/Ge sputtered Si substrates were loaded into a stainless steel micro reactor cell connected by metal tubing. The reaction cell and connections were dried for 24 h at 180 ^{o}C under vacuum. A DPG solution was loaded into a Hamilton GASTIGHT$^{(R)}$ sample-lock syringe (1000 series) inside a nitrogen filled glovebox under stringent precautions against water. Prior to DPG injection, the coated Si substrate was annealed for 30 min at 430 ^{o}C (well above the nominal Au/Ge eutectic temperature) under flowing H_2/Ar (flow rate of 0.5 ml min^{-1}) atmosphere inside a tube furnace. The precursor solution was then injected into the metal reaction cell using a high precision syringe pump at a rate of 0.025 ml min^{-1}. H_2/Ar flow was maintained during the entire growth period. Typical growth times were 25 min, though the times were varied to study the effect on nanowire length. The

cell was allowed to cool down to room temperature and disassembled to access the growth substrate. Nanowires were washed with dry toluene and dried under N_2 flow for further characterization.

Structural characterization was carried out using scanning electron microscopy (SEM), transmission electron microscopy (TEM), energy dispersive X-ray (EDX) analysis and selective area electron diffraction (SAED). SEM was carried out on a FEI Quanta FEG 650 operating at 5-10 kV. Bright-field TEM, in-situ temperature dependent studies and SAED were carried out on a JEOL JEM 2100 transmission electron microscope operating at 200 kV, while EDX was carried out using an Oxford Instruments INCA energy system fitted to the TEM. For TEM characterization, wires were dispersed in isopropanol and dropped onto lacey carbon 400 mesh copper grids. Bilayer and nanowire cross-sections were performed on a FEI Helios Nanolab^{TM} dual-beam SEM/FIB suite using a standard lift-out technique similar to that described elsewhere [30].

Results and Discussion

Figure 1(a) presents a schematic of the nanowire growth process using a 2-part Si substrate consisting of a Au (5 nm) and Au/Ge (5 nm/*x* nm) bilayer film, with varying Ge thickness (*x* = 1, 2, 5 nm) (shown in the inset in figure 1(b)). A cross-sectional TEM image of a pre-annealed Au/Ge (5 nm/1 nm) bilayer film deposited on a Si(100) substrate is shown in figure S1 (see Supporting Information). The presence of a 3-4 nm SiO_2 layer beneath the Au film prevents the direct interaction of Au with the underlying Si substrate and the subsequent formation of a Au/Si alloy upon annealing, as previously reported by Ferallis *et al.* [31]. Significantly, this SiO_2 layer remains intact after annealing at 430 ^{o}C for 30 min (see Supporting Information, figure S1(b)), confirming the absence of intermixing between the Au films and the Si substrates.

The bulk phase diagram for the Au/Ge binary system (figure 1(b)) [32] traces the progression of an Au/Ge binary alloy system from a solid Au film to Ge nanowire growth, as the concentration of the Ge component in the two-phase system increases. The phase diagram, in conjunction with the

schematic shown in figure 1(a), can be used to explain the participation of the Ge film to yield high aspect ratio nanowires. Typically, VLS growth requires the presence of both a semiconductor material and a metal catalyst to form a binary alloy before nanowire growth can proceed. A typical VLS process involves a Au catalyst heated above the eutectic point of the metal-semiconductor binary system, for example, 360 ^{o}C with a 28 % uptake of Ge in Au [32]. Without any Ge uptake, the binary system remains at the beginning of regime I on the red line of the phase diagram, as shown in figure 1(b), *i.e.* to the far left of the Au rich region (with 0 % Ge content). As the system is heated to the synthesis temperature, Au on the bilayer part of the Si substrate is exposed to Ge, forming a eutectic liquid melt catalyst with a certain uptake of Ge (regime II, figure 1(b) and part II, figure 1(a)) whilst the pure Au part of the substrate remains unexposed to Ge. With an increased supply of Ge from the precursor, the alloy particle becomes supersaturated causing solid Ge to crystallize out of the droplet forming a nanowire (regime III, figure 1(b)). The incubation time associated with Ge nucleation is directly related to the Ge supersaturation ($\Delta\mu$), *i.e.* the difference in the chemical potential between Ge in the Au/Ge alloy and Ge in the crystalline nanowire. Hence, a reduced incubation time for nanowire nucleation can be achieved by increasing the solute concentration in a two phase liquid alloy and thus the supersaturation of the Ge in the binary catalyst system [33].

Exposure of the Au/Au-Ge substrate to the Ge precursor (DPG), results in a higher Ge supersaturation in the Au/Ge bilayer film (regime III, figure 1(b)), and faster nucleation of Ge nanowires, as seen in part III of figure 1(a). The Au side of the substrate however only reaches regime II in the phase diagram with the introduction of DPG into the reaction chamber. Sustained flow of the Ge precursor through the system results in further growth of the nanowires on the Au/Ge substrate side, as the system is already in the Ge-rich part of the phase diagram (part IV of the schematic in figure 1(a)). At the same time interval, the Au side reaches regime III of the phase diagram in figure 1(b) and nucleation of solid Ge occurs. Consequently, Ge nanowires grow first on the Au/Ge bilayer side due to a lower induction time, resulting from faster supersaturation and nucleation of the catalytic seeds. Hence, the bilayer system produces longer wires when compared

with standard Au seed mediated growth methods over a typical growth period of 25 min (figures 2(a) and (b)). Millisecond timescales for a single nucleation events have previously been predicted through a time resolved simulation study of a VLS-nanowire growth process [34]. However, monitoring the time scales of single nucleation events in a 2D layer-by-layer growth process on both the Au and Au/Ge bilayer sides of a substrate was beyond our experimental capability. Hence a 25 min time interval was chosen to compare multiple nucleation events in both the Au and Au/Ge bi-layer films, which collectively contribute to the nanowire growth process [33,35].

Figures 2(a) and (b) show top-down SEM images of Ge nanowires grown from a Au film and a Au/Ge bilayer film (5 nm/2 nm) respectively, using the LICVD methodology at 430 ^{o}C with a 25 min growth time. SEM analysis supports the argument outlined above for a faster supersaturation rate and hence a higher growth rate of nanowires with the Au/Ge film (where the Ge film is 2 nm), by revealing significantly longer wires on the Au/Ge side (7.7 ± 3.0 μm) of the substrate when compared to the Au side (2.7 ± 0.8 μm) for a typical growth time of 25 min (figure 2(e)), corresponding to growth rates of 4.9×10^{-3} and 1.8×10^{-3} μm s^{-1} for growth on the Au/Ge and Au side respectively. The calculated nanowire growth rates include a contribution from the incubation time in the nucleation mediated process. The significantly longer nanowire lengths can also be seen in the insets of both figures 2(a) and (b), which show SEM images of nanowires tilted 90 degrees to the beam, grown on the Au and Au/Ge bilayer side of the Si substrate respectively. SEM characterization confirmed a high abundance of nanowires on the substrate. A sharp interface can be seen between the Au and Au/Ge sides of a substrate shown in figure 2(c), highlighting the presence of different growth regimes on the two sides and that as the interface is crossed, the growth regime rapidly changes. The inset in figure 2(c) shows a photograph of the substrate after removal from the reaction cell. The interface (marked by the red arrow) between the different growth regimes on the Au and Au/Ge sections of the substrate can clearly be seen in the photograph. Figure 2(d) shows a high resolution TEM micrograph of a Ge nanowire grown on the Au/Ge bilayer side of a Si substrate, highlighting the crystallinity of the nanowire. The inset in figure 2(d) is an SAED pattern

imaged along the [110] zone axis of the nanowire, confirming its cubic crystal structure (PDF 04-0545) and [111] growth direction. Nanowires grown from the Au/Ge and Au-only layers were found to have predominantly [110] or [111] growth directions, with the [110] direction prevalent for nanowires with diameters below 25-30 nm, as previously reported by Schmidt *et al.*[36] for Si nanowires (see Supporting Information, figure S3). These growth orientations do not agree with the recently published data of Dayeh *et al.* who reported [111] growth directions for nanowires below 25 nm[17]. Only a minority of our Ge nanowires with diameters below 25 nm, had a [111] growth orientation. Figure S2 (see Supporting Information) presents additional high resolution TEM images of Ge nanowires grown from the two-part substrate in order to highlight the uniform morphology of the nanowires. Recently, Han *et al.* [37] demonstrated that tuning the catalytic composition of binary alloys affected the crystallographic growth direction of GaAs nanowires produced. Hence, the diameters and growth directions of over 60 nanowires were compiled for both the Au and Au/Ge growth regimes. Distributions of Ge nanowire growth directions from the Au and Au/Ge sides of Si substrates revealed predominantly [110] and [111] orientations on both sides. On the Au side, approximately 69 % of the nanowires adopted a [111] orientation while 24 % have a [110] direction. A minority of the nanowires examined adopt a [211] orientation (6 %). A larger percentage of the Ge nanowires examined on the Au/Ge side had a [111] orientation, with 83 % of them adopting this growth direction, while only 15 % adopted the [110] orientation. Again, a minority of wires had a [211] growth direction (> 2 %) (see Supporting Information, figure S3). Hence, the addition of a Ge buffer layer did not notably influence the overall nanowire growth direction. Au/Ge bilayer films can therefore be utilized to generate high-quality Ge nanowires without sacrificing orientation uniformity. Additionally, the diameter of the Ge nanowires grown from the Au/Ge side were similar to those synthesized on the Au side, with mean diameters of 49.1 ± 14.6 nm and 42.1 ± 11.2 nm for the Au side and Au/Ge bilayer side respectively. Whilst an in-depth investigation into the nanowire orientation dependence on length was not undertaken in this study, figure S3 (see Supporting Information) infers that the majority of the long nanowires adopted a [111] orientation, assuming a supersaturation limited growth process and the Gibbs-Thomson effect.

Figure 3(a) shows a histogram of the length distributions of Ge nanowires grown from Au/Ge bilayer films with increasing Ge film thickness. In all cases, a 2-part substrate described in figure 1 was used, allowing a direct comparison between nanowire growth on the Au and Au/Ge sides of the substrate under identical reaction conditions. The histogram shows the lengths of Ge nanowires grown from a standard Au film (5 nm) and from Au/Ge bilayer films with Ge thicknesses of 1, 2 and 5 nm. Each plot consists of a Lorentzian fit in addition to the raw data, which was obtained by direct measurement of nanowire lengths using TEM. As evident from the graph, as the thickness of the Ge layer increased, so did the mean length of the nanowires, accompanied by a broadening of the length distribution. The mean lengths in each case were found to 2.7 ± 0.8 μm, 5.5 ± 2.3 μm, 7.7 ± 3.0 μm and 9.02 ± 3.54 μm for the pure Au film and Au/Ge bilayer films with a Ge thickness of 1, 2 and 5 nm respectively. A distinct broadening in the length distribution of the nanowires with increasing Ge thickness is apparent from the Lorentzian fits shown in figure 3(a). The FWHM increased from 0.8 to 3.5 μm for Ge nanowires grown from a Au-only film to a 5 nm Au/5 nm Ge bilayer film and can be explained by the difference in the supersaturation and nucleation kinetics for the eutectic binary alloy seeds compared to Au. A Au/Ge bilayer creates a binary alloy upon annealing, prior to any precursor injection. However, the binary alloy particles do not contain an equal Ge concentration, as the distribution of the Ge layer within the Au is not uniform. The percentage of Ge is not the same in each binary alloy particle catalyst, resulting in different levels of supersaturation. Consequently, when the Ge precursor is injected, nucleation of Ge at the TPB will not occur simultaneously for all binary alloy particles, resulting in a broad distribution of lengths. The broadening increases with thicker Ge films, yielding Au/Ge binary alloy particles with a higher and varied Ge content. With the pure Au film, there is no formation of binary alloy particles after annealing. The Au islands which form upon nucleation are exposed to the Ge precursor in roughly equal proportions, resulting in near equal supersaturation and simultaneous nucleation of Ge nanowires, yielding a narrower length distribution. SEM micrographs (shown in the inset in figure 3(a)) of Ge nanowires grown from a Au layer, a Au (5 nm)/Ge (2 nm) bilayer and a Au (5 nm)/Ge (5

nm) bilayer show longer nanowires with increasing Ge film thickness, *i.e.* increasing Ge content in the eutectic catalyst. As mentioned previously, the formation of a Au/Si alloy as a result of the intermixing between the Au and Si substrate upon annealing is unlikely due to the presence of a 3-4 nm SiO_2 layer. To further alleviate concerns about intermixing, we carried out growth experiments on Si/SiO_2 wafers (200 nm SiO_2 layer). Figure S4(a) (see Supporting Information) shows a TEM micrograph of a cross-section of one of these substrates with a deposited Au/Ge bi-layer. The 200 nm SiO_2 layer is clearly visible. Figure S4(b) reveals a nanowire length distribution very similar to that shown in figure 3(a) for a 2 nm Ge film, suggesting that Au/Si intermixing was not an issue in our experiments.

Figure 3(b) shows a second histogram of nanowire growth rates from the same bilayers as shown in figure 3(a). As expected, the overall nanowire growth rate increases with the thickness of the Ge layer, due to the raised Ge concentration in the binary alloy particle catalysts, inferring a faster nucleation of Ge at the TPB. The overall nanowire growth rate can be separated into constituent parts: (i) the rate of incubation, *i.e.* the time required for the initial nucleation to take place upon precursor injection and (ii) the rate after incubation. The incubation time consists of a dead time (T_1), *i.e.* the time for the precursor to travel from the source chamber to reaction chamber and the time for a nucleation event to occur (T_2). As a millisecond timescale is expected for a single nucleation event, shortening of the dead time in the Au/Ge bi-layer contributes towards a faster overall incubation rate ($T_1 + T_2$). During this dead time, the Au side remains inert in terms of germination and nucleation. However, on the Au/Ge side, the nucleation process can initiate due to the presence of the Ge film, effectively minimizing the dead time. In other words, single nucleation events take longer on the Au side because of the added dead time.

The faster nucleation of Ge with increasing Ge film thickness is explained with a magnified representation of the eutectic region of the bulk phase diagram (figure 3(c)). Annealing of the Au and Au/Ge films prior to nanowire growth is the key to obtaining favorable growth kinetics with a

Ge buffer layer. The sintering process creates binary alloy catalysts which participate in the growth process, thus yielding a higher Ge concentration when compared to standard Au seeds. Increasing the Ge concentration corresponds to progression along the horizontal dashed red line in figure 3(c), representing nanowire growth at a temperature of 430 ^{o}C. Position I on the partial bulk Au/Ge phase diagram (figure 3(c)) represents 0 % Ge in a Au/Ge alloy and is analogous to using a pure Au film. Assuming the absence of a Ge precursor, the Au film does not form a Au/Ge alloy upon annealing at our growth temperature prior to nanowire growth. Introducing Ge into the film moves the Au/Ge system along the dashed red line to regime II which, assuming complete intermixing, is analogous to a 5 nm Au/1 nm Ge bilayer film, or approximately 14 at.% Ge in the Au/Ge binary alloy. Here, the system will form a Au/Ge liquid mixture with solid Au upon heating, but the entire film will not form a liquid alloy and the solid Au will require an incubation time for supersaturation to occur. A further increase in the Ge concentration in the Au/Ge system to a composition of 26 at.% (regime III) places the system within the liquid region of the phase diagram and forms a Au/Ge binary eutectic alloy. This is analogous to the participation of a 5 nm Au/2 nm Ge bilayer film. Finally, increasing the thickness of the Ge film in the Au/Ge bilayer to 5 nm (47 at.% Ge in the Au/Ge alloy) moves the Au/Ge binary system further along the dashed red line to point IV, into the Ge-rich region of the phase diagram, resulting in extremely fast nucleation. Although the bulk binary phase diagram has been used to explain the nanowire growth scenario, a shift in the liquidus and solidus curve in the bulk phase diagram should be taken into account due to nanoscale size effects[17, 38-40].

Figure S5 (see Supporting Information) summarizes the dependence of nanowire length and growth rate on Ge buffer layer thickness. The nanowire growth after incubation, *i.e.* independent of T_1 and T_2, is also influenced by the introduction of a Ge layer to the Au-coated substrate, as evidenced from the nanowire length distribution plots shown in figure S6 (see Supporting Information), for Ge nanowire growth from Au and Au/Ge substrates for different reaction times. A more pronounced increase in the mean length of the nanowires in the Au/Ge side for different reaction period indicates a change in the growth rate during and after nanowire incubation.

Supersaturation acts as a thermodynamic driving force which transfers Ge atoms from a seed particle to a nanowire. Givargizov presented a quadratic relationship between the growth rate of Si nanowires and the supersaturation according to equation 1 [20]:

$$v = b\left(\frac{\Delta\mu}{kT}\right)^2 \quad (1)$$

where v is the nanowire growth rate, b is the kinetic coefficient of crystallization, $\Delta\mu$ is the supersaturation and kT is the Boltzmann distribution. According to equation 1, the growth rate can be enhanced by increasing the supersaturation. Moreover, the supersaturation increases with Ge concentration according to equation 2 [17]:

$$\Delta\mu = kT\ln\left(\frac{C}{C_{eq}}\right) \quad (2)$$

where C is the solute concentration in the liquid binary alloy and C_{eq} is the equilibrium solute concentration determined from the bulk phase diagram. Thermodynamically, increasing the Ge concentration in the seed is associated with increasing the chemical potential of the growth species in solution, thus increasing the driving force responsible for nanowire growth. In this study, the Ge solute concentration (C) has been increased by adding a Ge layer onto a Au film and annealing the substrate to form a binary Au/Ge alloy prior to the introduction of the Ge precursor. Increasing the thickness of the Ge layer further increases C (assuming rapid intermixing) and hence raises the supersaturation to a greater extent. The exponential dependence of the nanowire growth rate on the Ge concentration in the binary alloy catalyst (figure 3(d)) can be inferred from equations (1) and (2), which further confirms the dependence of nanowire growth rate on the supersaturation. Considering 2D ledge nucleation at the TPB for Ge nanowire growth, the kinetic barrier for nucleation, as derived from classical nucleation theory, is given in equation 3 [33]:

$$\Delta G_B = \alpha^2 / 4\Delta\mu \quad (3)$$

where α is a geometrically weighted coefficient for forming a new surface and ΔG_B is the kinetic barrier for Ge ledge nucleation at the TPB. The size of ΔG_B determines the rate of Ge nucleation at the TPB and thus the overall growth rate of the Ge nanowires. ΔG_B can be related to the rate of nucleation according to equation 4 below:

$$P(t) = K \exp\left(-\frac{\Delta G_B}{k_b T}\right) \quad (4)$$

where K can be represented by $ZC\omega$, in which Z is the Zeldovich factor, C is the monomer concentration and ω is the molecular attachment frequency [33]. As the supersaturation increases, the rate of nucleation increases according to $exp\left(-\frac{b}{\Delta\mu}\right)$. An increased rate of nucleation also means a lower induction time.

Nucleation of Ge from a binary seed occurs within two different growth regimes over two time-scales [41]. The first of these is τ_{Ge} which represents the time for Ge nucleation to occur at the triple phase boundary (TPB) and the second is $\tau_{Au,}$ representing the time needed to add enough Ge to dissolve all the Au and melt the particle. In a standard VLS method with a Au film, usually $\tau_{Au} << \tau_{Ge}$ which tells us that the Au seed melts to form a AuGe alloy much faster than the nucleation of Ge to form a nanowire. This is logical as moving from left to right across the phase diagram (figure 1(b)), the Au/Ge binary system reaches the liquid alloy region before progressing on towards the nucleation region on the Ge rich side. However, upon increasing the Ge concentration in the binary alloy particles, by using an Au/Ge bilayer film instead of a Au film, the time for the particle melting (τ_{Au}) can be further reduced by shortening the time required for overall nucleation. Specifically, if

the time required for the system to progress across the alloying (liquid) region of the phase diagram is shortened, then it can reach the nucleation stage quicker. This argument can be supported mathematically, leading to a direct dependence of the Ge solute concentration on induction time, as $\tau_{Ge} \propto (-aC)$, where τ_{Ge} is the induction time for nucleation (reciprocal of the nucleation rate *P(t)*), *C* is the Ge solute concentration and *a* is a constant for a set of certain experimental parameters. The nanowire growth rate takes into account multiple nucleation events and lateral crystal evolution. The enhanced Ge supersaturation on the Au/Ge bi-layer part of the substrates increases the nucleation rate for each step and hence when all of these nucleation events are added together, an overall faster nanowire growth rate is obtained for the Au/Ge bi-layers. The nucleating cycle completes with the liquid alloy drop rejecting the excess Ge to reach an equilibrium state. Length distribution curves for the growth at different time scales (15, 25 and 40 min) show different nanowire growth rates (actual growth rate excluding the incubation time) for Au and Au/Ge sides of Si substrates (see Supporting Information, figure S6).

The Ge nucleation kinetics for bilayer films of varying Ge layer thickness was further investigated using *in-situ* annealing experiments inside a TEM. Au and Au/Ge bilayer films were deposited on SiO_2 supported films with thicknesses identical to those used to synthesize Ge nanowires. As in-situ TEM allows the examination of nanoscale systems as they undergo physical transformation (upon heating, for example), insights into the liquid-solid interface behaviour, phase nucleation and the mechanisms controlling nucleation and growth [42-44] can be obtained. Figure 4 shows a series of dark-field TEM images taken during in-situ heating of the Au-only and Au/Ge bilayer films. Dark-field imaging was used to eliminate contrast due to mass/thickness allowing comparison between alloying of the bilayer films. Figure 4(a) represents a series of images taken during the in-situ heating of a 5 nm Au film. The bright spots represent the diffraction contrast from solid crystalline Au with specific orientations that meet the Bragg condition. A significant contrast can be observed across the entire temperature range, as the Au does not form an alloy and remains crystalline even at high temperatures. Conversely, figures 4(b) and (c) show a reduction in diffraction contrast as the

temperature increases for the 5 nm Au/1 nm Ge and 5 nm Au/5 nm Ge bilayers films respectively. This change in diffraction is particularly significant in figure 4(c) where the contrast completely disappears at high temperatures leaving uniform grey particles, inferring the complete formation of a liquid alloy; each sample was heated for 45 min in total with each temperature investigated maintained for 5 min. This in-situ data clarifies the fact that thinner Ge films, *i.e.* lower Ge concentration, take longer to alloy with Au than thicker films. Hence, longer nanowires are seen for thicker Ge films.

Higher magnification images were taken of the particles at high temperatures and at room temperature to compare the morphology of the particles before and after annealing of the films for different Ge film thicknesses. Moreover, the solidification of the particles and phase separation of the semiconductor material from the metallic material were compared. These studies offer an insight into the nucleation kinetics of Ge for varying Ge film thicknesses. Figure 5(a) shows a TEM image of a 5 nm Au/5nm Ge bilayer film above the eutectic temperature during in-situ heating. Alloy particles in their liquid state are formed at this temperature as confirmed by the uniform contrast of the islands. After the sample was cooled down to room temperature, precipitation of Ge occurred as the particles solidify, as shown in figure 5(b). In comparison to figure 5(a), there was a sharp contrast between the Au and Ge segments which is indicative of solidification and segregation of the semiconductor phase from the metallic phase. As a consequence of this solidification, there is a shrinking of particle volume, which is confirmed by the bar chart shown in figure 5(c). This bar chart represents the projected areas taken of the dark Au portion of each particle; the Ge portion is excluded as Ge has been expelled from the Au due to phase separation. The areas of 15 particles were taken before and after cooling to room temperature during in-situ TEM studies and plotted. As is evident from figure 5(c), the mean particle size decreased upon cooling, a result which can more easily be seen in the distribution shown in the inset (lorentzian curves). Figure 5(d) shows a TEM image of the area within the red box in figure 5(b) and highlights the sharp contrast between the Au and Ge phases. The red lines mark the edge of the particles and the interface between the two

phases. It should be noted that the difference in contrast cannot be due to thickness, as these sharp contrast differences would also be seen at high temperatures (figure 5(a)), if this was the case. Figures S7 and S8 (Supporting Information) present a similar analysis for the 5 nm Au/1 nm Ge bilayer film and Au film respectively. Comparing part (c) in figures 5, S7 and S8, the difference in particle sizes above the eutectic temperature and after cooling to room temperature becomes less significant as the thickness of the Ge film is reduced. The difference in particle sizes for the pure Au film (see Supporting Information, figure S8) is negligible because Ge is obviously absent and so the particles remain solid at high temperature and during cooling (as is evident from the diffraction contrast throughout figure 4(a)). The mismatch in sizes between the particles at 800 ºC and room temperature gradually becomes more significant with thicker Ge layers (see Supporting Information, figure S9). This observation is reasonable due to the higher content of the Ge component in the eutectic binary alloy particles for the bilayer film with thicker Ge layers. Also the interface between the Au and Ge after cooling to room temperature is less discernible in the TEM micrographs for the Au (5nm)/Ge (1nm) films due to weaker contrast between the two phases (see Supporting Information, figures S7 and S8). In-situ TEM annealing experiments with Au and Au/Ge films produced significant insights into the formation of eutectic binary alloy seeds and contribution of higher Ge supersaturation in the nucleation process.

Conclusion

To conclude, a novel method of tailoring the supersaturation of the Au/Ge binary alloy system has been utilized to grow long, crystalline Ge nanowires. Au/Ge bilayer films were successfully demonstrated to increase the Ge solute concentration in the alloy seed and hence the supersaturation before the injection of a Ge precursor for nanowire growth. Nanowires were collected on a two-part substrate consisting of a Au/Ge bilayer and a Au-only film which allowed the comparison of growth dynamics under identical conditions. Lengths and growth rates were found to be greater on the Au/Ge side while growth directions and diameter were consistent on both sides. In-situ TEM was used to clarify the growth characteristics via diffraction contrast, thus enabling the comparison of the

alloying procedure for the different bilayers. This unique method marks the first time a metal-semiconductor binary alloy has been used to manipulate the Ge nucleation kinetics at the triple phase boundary during nanowire growth. This approach of manipulating supersaturation with a change in the solute concentration in the alloy seed could be combined with the other critical growth kinetics influencing parameters, *i.e.* pressure, temperature, dopant concentration, precursor decomposition chemistry, equilibrium concentration *etc*. to realize an ideal scenario for much improved growth maneuvering in nanowires. Our method opens up the possibility of engineering the growth of nanowires, thus allowing the tuning of nanowire properties for future nanowire devices.

Acknowledgements

We acknowledge financial support from the Irish Research Council and Science Foundation Ireland (Grants: 09/SIRG/I1621, 06/IN.1/I106, 08/CE/I1432 and 09/IN.1/I2602). This research was also enabled by the Higher Education Authority Program for Research in Third Level Institutions (2007-2011) via the INSPIRE programme.

Associated Content

Supporting Information. Further high resolution TEM micrographs highlighting the monocrystallinity and uniform growth direction of our nanowires, SEM images of the annealed Au and AuGe films, growth direction statistics and additional in-situ data. This material is available free of charge via the internet at http://pubs.acs.org

References

1. Cui, Y.; Lieber, C. *Science* **2001,** 291, 851.
2. Huang, Y.; Lieber, C. *Pure. Appl. Chem.* **2004,** 76, 2051.
3. Barth, S.; Hernandez-Ramirez, F.; Holmes, J. D.; Romano-Rodriguez, A. *Prog. Mater. Sci.* **2010,** 55, 563.
4. Heath, J.; LeGoues, F. *Chem. Phys. Lett.* **1993,** 208, 263.
5. Tuan, H. Y.; Lee, D. C.; Hanrath, T.; Korgel, B. A. *Chem. Mater.* **2005,** 17, 5705.
6. Petkov, N.; Birjukovs, P.; Phelan, R.; Morris, M.; Erts, D.; Holmes, J. *Chem. Mater.* **2008,** 20, 1902.
7. Lu, X. M.; Fanfair, D. D.; Johnston, K. P.; Korgel, B. A. *J. Am. Chem. Soc.* **2005,** 127, 15718.
8. Andzane, J.; Petkov, N.; Livshits, A. I.; Boland, J. J.; Holmes, J. D.; Erts, D. *Nano Lett.* **2009,** 9, 1824.
9. Ziegler, K. J.; Lyons, D. M.; Holmes, J. D.; Erts, D.; Polyakov, B.; Olin, H.; Svensson, K.; Olsson, E. *Appl. Phys. Lett.* **2004,** 84, 4074.
10. Chockla, A. M.; Klavetter, K. C.; Mullins, C. B.; Korgel, B. A. *ACS Appl. Mater. Inter.* **2012,** 4, 4658.
11. Seo, M. H.; Park, M.; Lee, K. T.; Kim, K.; Kim, J.; Cho, J. *Energy Environ. Sci.* **2011,** 4, 425.
12. Chan, C. K.; Zhang, X. F.; Cui, Y. *Nano Lett.* **2008,** 8, 307.
13. Burchhart, T.; Lugstein, A.; Hyun, Y. J.; Hochleitner, G.; Bertagnolli, E. *Nano Lett.* **2009,** 9, 3739.
14. Garfunkel, E.; Mastrogiovanni, D.; Klein, L.; Wan, A.; Du Pasquier, A. *Abstr. Pap. Am. Chem. S.* **2008,** 236.
15. Nguyen, P.; Ng, H.; Meyyappan, M. *Adv. Mater.* **2005,** 17, 549.
16. Cullis, A.; Canham, L.; Calcott, P. *J. Appl. Phys.* **1997,** 82, 909.
17. Dayeh, S. A.; Picraux, S. *Nano Lett.* **2010,** 10, 4032.
18. Givargizov, E. I., *Highly anisotropic crystals*. D Reidel Pub Co: 1987; Vol. 3.
19. Kodambaka, S.; Tersoff, J.; Reuter, M.; Ross, F. *Phys. Rev. Lett.* **2006,** 96, 96105.
20. Givargizov, E. I. *J. Cryst. Growth* **1975,** 31, 20.
21. B Lewis; Anderson, J. S., *Nucleation and Growth of Thin Films*. Academic, New York: 1978.
22. Han, N.; Wang, F.; Hou, J. J.; Yip, S. P.; Lin, H.; Fang, M.; Xiu, F.; Shi, X.; Hung, T. F.; Ho, J. C. *Cryst. Growth. Des.* **2012,** 12 6243.
23. Xu, H.; Wang, Y.; Guo, Y.; Liao, Z.; Gao, Q.; Jiang, N.; Tan, H. H.; Jagadish, C.; Zou, J. *Cryst. Growth. Des.* **2012,** 12, 2018.
24. Kim, B.-S.; Kim, M. J.; Lee, J. C.; Hwang, S. W.; Choi, B. L.; Lee, E. K.; Whang, D. *Nano Lett.* **2012,** 12, 4007.
25. Hannon, J.; Kodambaka, S.; Ross, F.; Tromp, R. *Nature* **2006,** 440, 69.
26. Kim, J. H.; Moon, S. R.; Yoon, H. S.; Jung, J. H.; Kim, Y.; Chen, Z. G.; Zou, J.; Choi, D. Y.; Joyce, H. J.; Gao, Q.; Tan, H. H.; Jagadish, C. *Cryst. Growth. Des.* **2012,** 12, 135.
27. Jung, J. H.; Yoon, H. S.; Kim, Y. L.; Song, M. S.; Kim, Y.; Chen, Z. G.; Zou, J.; Choi, D. Y.; Kang, J. H.; Joyce, H. J.; Gao, Q.; Hoe Tan, H.; Jagadish, C. *Nanotechnology* **2010,** 21, 295602.
28. Jung, S. J.; Lutz, T.; Boese, M.; Holmes, J. D.; Boland, J. J. *Nano Lett.* **2011,** 11 1294.
29. Jung, S. J.; Lutz, T.; Bell, A. P.; McCarthy, E. K.; Boland, J. J. *Cryst. Growth. Des.* **2012,** 12, 3076.
30. Giannuzzi, L. A.; Stevie, F. A. *Micron* **1999,** 30, 197.
31. Ferralis, N.; Maboudian, R.; Carraro, C. *Journal of the American Chemical Society* **2008,** 130, 2681.
32. http://www.crct.polymtl.ca/fact/documentation/SGTE/, In.
33. Gamalski, A.; Ducati, C.; Hofmann, S. *J. Phys. Chem. C* **2011,** 115, 4413.
34. Eisenhawer, B.; Sivakov, V.; Christiansen, S.; Falk, F. *Nano Letters* **2013,** 13, 873.
35. Dubrovskii, V.; Xu, T.; Lambert, Y.; Nys, J. P.; Grandidier, B.; Stiévenard, D.; Chen, W.; Pareige, P. *Physical review letters* **2012,** 108, 105501.
36. Schmidt, V.; Senz, S.; Gosele, U. *Nano Lett.* **2005,** 5, 931.
37. Han, N.; Wang, F.; Hou, J. J.; Yip, S. P.; Lin, H.; Fang, M.; Xiu, F.; Shi, X.; Hung, T. F.; Ho, J. C. *Crystal Growth & Design* **2012,** 12, 6243.
38. Sutter, E. A.; Sutter, P. W. *ACS Nano* **2010,** 4, 4943.
39. Sutter, E.; Sutter, P. *Nano Lett.* **2008,** 8, 411.
40. Adhikari, H.; Marshall, A.; Goldthorpe, I.; Chidsey, C.; McIntyre, P. *ACS Nano* **2007,** 1, 415.

41. Kim, B. J.; Wen, C. Y.; Tersoff, J.; Reuter, M. C.; Stach, E. A.; Ross, F. M. *Nano Lett.* **2012,** 12, 5867.
42. Woehl, T. J.; Evans, J. E.; Arslan, I.; Ristenpart, W. D.; Browning, N. D. *ACS Nano* **2012,** 6, 8599.
43. Ross, F. M. *Rep. Prog. Phys.* **2010,** 73, 114501.
44. Nikolova, L.; LaGrange, T.; Reed, B.; Stern, M.; Browning, N.; Campbell, G.; Kieffer, J.-C.; Siwick, B.; Rosei, F. *Appl. Phys. Lett.* **2010,** 97, 203102.

Figures

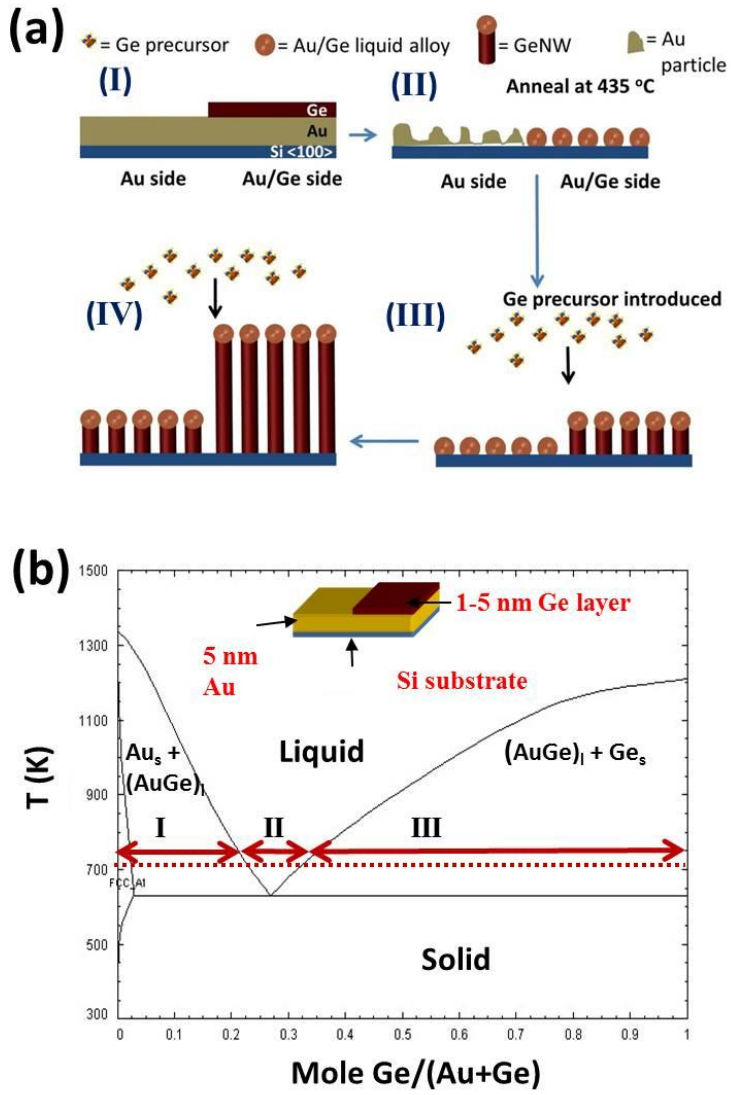

Figure 1. (a) Schematic illustrating the difference between Ge nanowire growth on the Au and Au/Ge bilayer side of a Si substrate. Nanowires grown on the bilayer side nucleate faster and thus have greater lengths than those on the Au side, for a given growth time. (b) Phase diagram of the Au/Ge alloy system tracing and comparing the evolution of Ge nanowires grown on the Au side and Au/Ge bilayer side of the substrate. Inset shows the 2-part substrate used which consists of a Au film on one side and a Au/Ge bilayer on the other side.

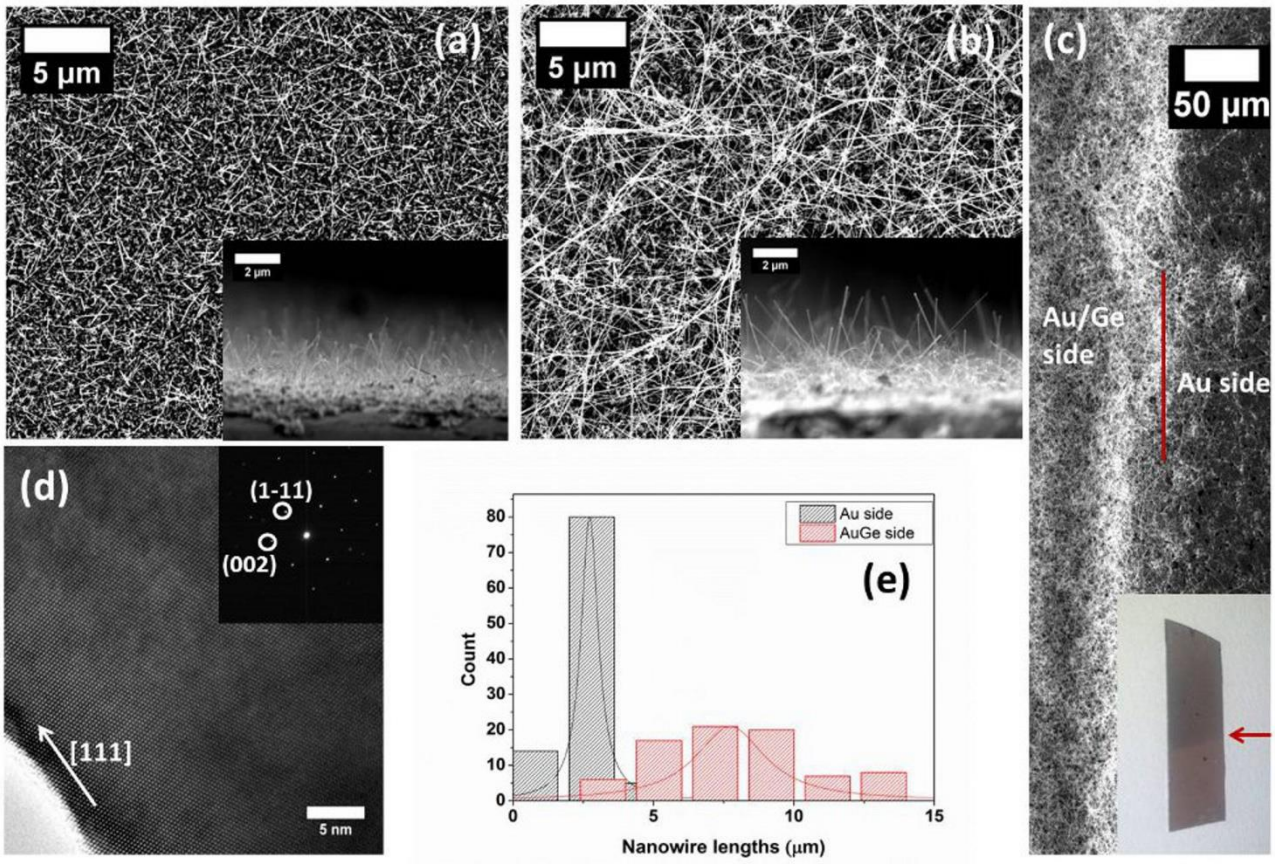

Figure 2. SEM and TEM images of Ge nanowires grown from a two-sided substrate. (a)-(b) Top-down SEM images showing Ge nanowires grown from the Au side and Au/Ge (5nm / 2 nm) side respectively; growth time was 25 min. Insets show cross-sectional SEM images of Ge nanowires on the Au side and Au/Ge side respectively. (c) Top-down SEM image showing the interface between the Au and Au/Ge side. Inset is a photograph taken of the substrate after removal from the CVD apparatus. The sharp interface implying different growth scenarios with the Au and Au/Ge film. (d) Lattice resolution TEM image of a Ge nanowires grown on the Au/Ge bilayer side. Inset is the SAED pattern viewed along the [110] zone axis which confirms the <111> growth direction. (e) Histogram confirming the significant difference in nanowire lengths between the Au and Au/Ge side. Lorentzian curves are fitted to both plots, which show a much broader size distribution of the GeNWs grown on the bi-layer side

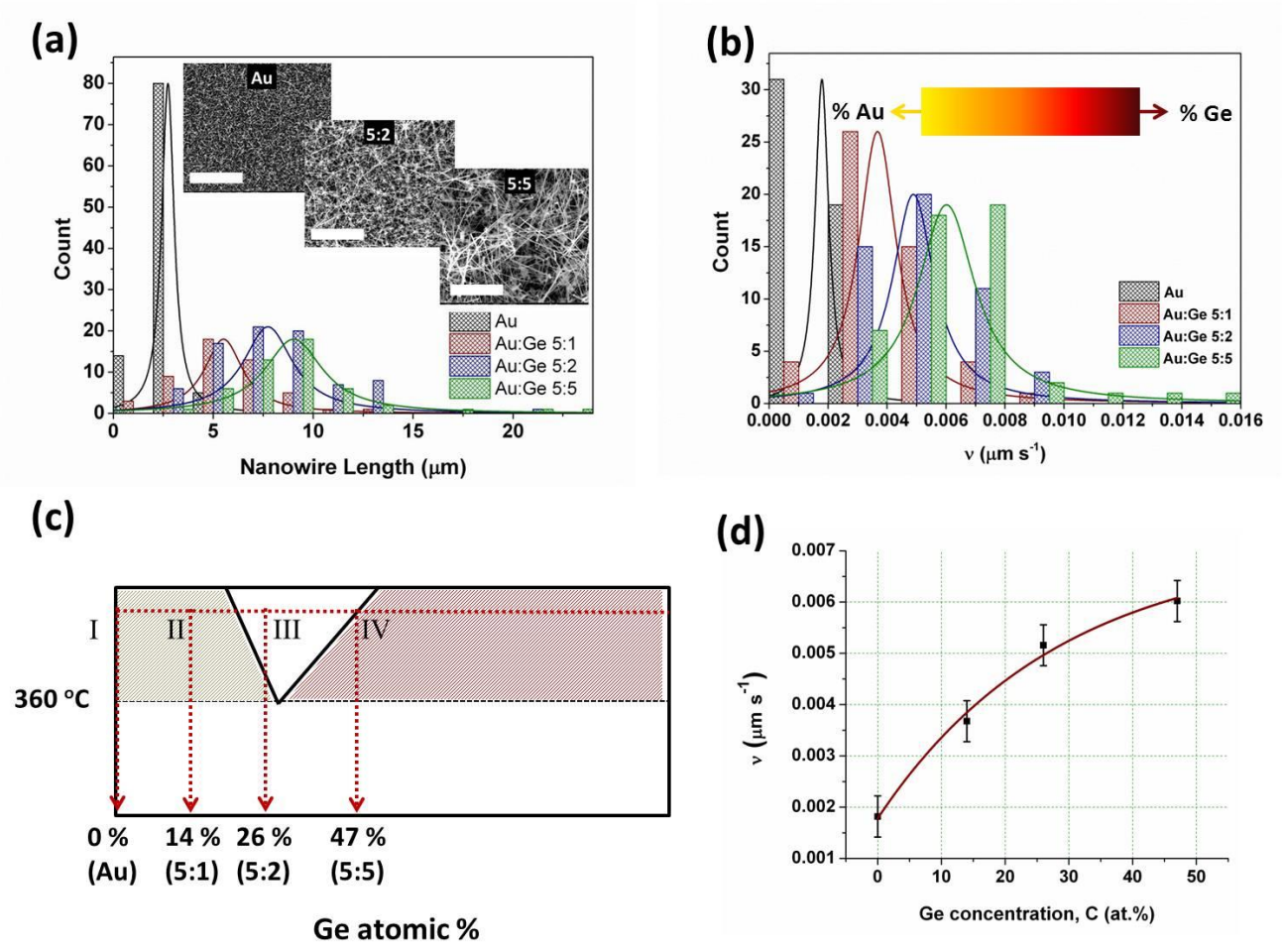

Figure 3. (a) Histogram showing the relative length distributions of Ge nanowires grown from a Au film and Au/Ge bilayers with varying Ge thicknesses. Growth time in all cases in 25 mins. Insets show SEM images of Ge nanowires grown from a Au film as well as Au/Ge bilayers, with Ge layer thickness of 2 and 5 nm. (b) Histogram showing the relative growth rate distributions of Ge nanowires grown from a Au film and Au/Ge bilayers with varying Ge thicknesses. Lorentzian curves are fitted to all plots in (a) and (b), and show a broadening of the size distribution in the length and growth rate of GeNWs as the thickness of the Ge film increases. (c) Enhancement of the low-temperature regime of the Au/Ge phase diagram shown in figure 1(b) which traces the behavior of the binary alloy formed from bilayers with increasing Ge solute concentration, *i.e.* increasing Ge film thickness. (d) Mean nanowire growth rate as a function of the Ge solute concentration in the binary alloy.

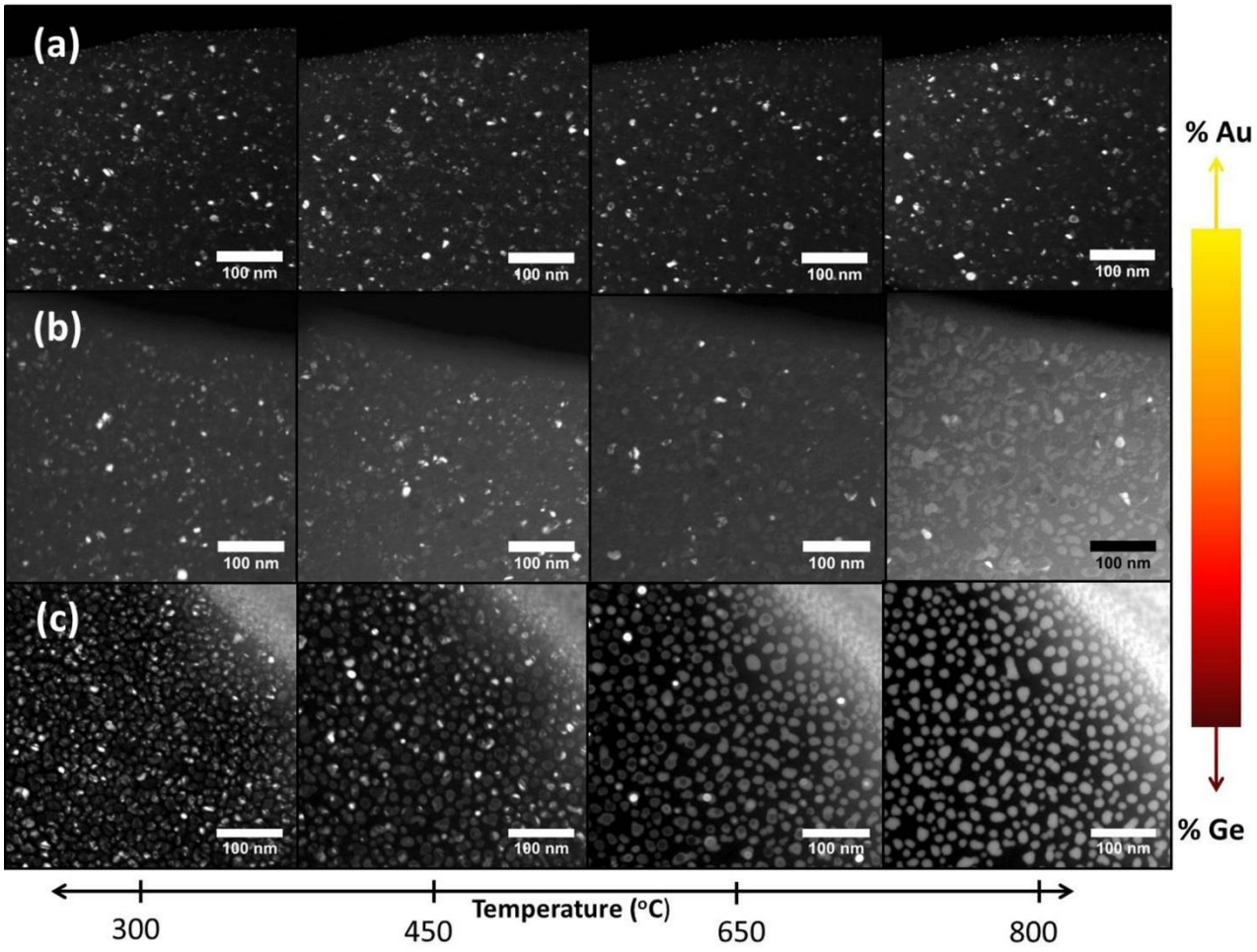

Figure 4. Three series of plan view dark field images showing the annealing of Au/Ge bilayer films deposited on SiO_2 membrane grids by in-situ TEM. Images show films at 300, 400, 650 and 800 °C. Heating of (a) a 5 nm Au film, (b) a 5 nm Au/1 nm Ge bilayer and (c) a 5 nm Au/5 nm Ge bilayer.

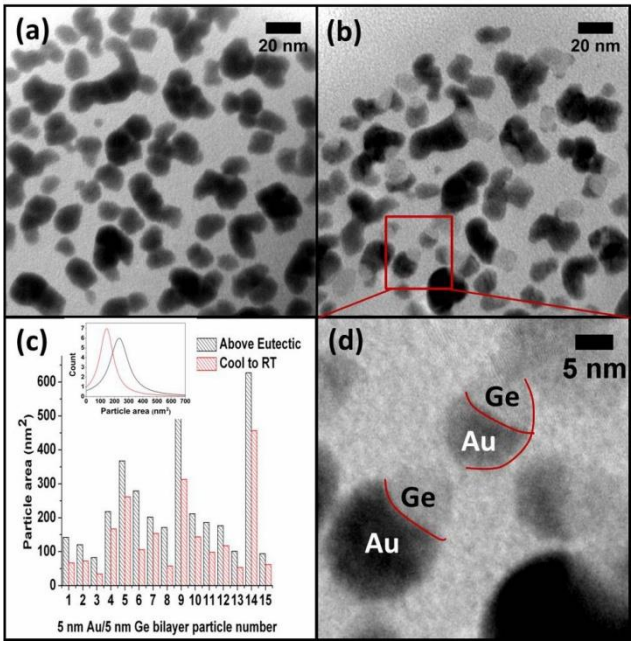

Figure 5. TEM analysis of Au/Ge alloy particles during in-situ temperature studies of the 5 nm Au/5nm Ge bilayer film. (a) TEM image of Au/Ge alloy particles above the eutectic temperature. (b) TEM micrograph of the Au/Ge particles shown in part (a) after cooling down to room temperature. (c) Bar chart showing the size differences between 15 particles measures above the eutectic temperature and after cooling to room temperature. Inset shows the Lorentzian curves of histograms plotted from the sizes of the same 15 particles at high temperature and after cooling to room temperature. (d) TEM image of the area inside the red box in (b), highlighting the separation of Ge from Au after cooling to room temperature. Red lines outline the interface between the Au and Ge.

Table of Contents Graphic